Simulation of Cooling and Pressure Effects on Inflated Pahoehoe Lava Flows

Lori S. Glaze[1] and Stephen M. Baloga[2]

[1]NASA GSFC

Lori.S.Glaze@nasa.gov

[2]Proxemy Research

sbaloga1@starpower.net

1 **Abstract:**

2 Pahoehoe lobes are often emplaced by the advance of discrete toes accompanied by inflation of

3 the lobe surface. Many random effects complicate modeling lobe emplacement, such as the

4 location and orientation of toe breakouts, their dimensions, mechanical strength of the crust,

5 micro-topography and a host of other factors. Models that treat the movement of lava parcels as a

6 random walk have explained some of the overall features of emplacement. However, cooling of

7 the surface and internal pressurization of the fluid interior has not been modeled. This work

8 reports lobe simulations that explicitly incorporate 1) cooling of surface lava parcels, 2) the

9 propensity of breakouts to occur at warmer margins that are mechanically weaker than cooler

10 ones, and 3) the influence of internal pressurization associated with inflation. The surface

11 temperature is interpreted as a surrogate for the mechanic strength of the crust at each location

12 and is used to determine the probability of a lava parcel transfer from that location. When only

13 surface temperature is considered, the morphology and dimensions of simulated lobes are

14 indistinguishable from equiprobable simulations. However, inflation within a lobe transmits

15 pressure to all connected fluid locations with the warmer margins being most susceptible to

16 breakouts and expansion. Simulations accounting for internal pressurization feature

17 morphologies and dimensions that are dramatically different from the equiprobable and

18 temperature-dependent models. Even on flat subsurfaces the pressure-dependent model

19 produces elongate lobes with distinct directionality. Observables such as topographic profiles,

20 aspect ratios, and maximum extents should be readily distinguishable in the field.

1. Introduction.

Numerous models with various degrees of complexity treat terrestrial and planetary lava flows as gravity-driven viscous or turbulent fluids on an inclined plane [e.g., *Nichols*, 1939; *Shaw and Swanson*, 1970; *Danes*, 1972; *Harrison and Rooth*, 1976; *Baloga*, 1987; *Baloga et al.*, 1995; *Baloga et al.*, 1998; *Harris and Rowland*, 2001; *Baloga et al.*, 2001; *Rowland et al.*, 2004; *Baloga and Glaze*, 2008; *Glaze et al.*, 2009; *Glaze et al.*, 2014]. These models consider the influence of large-scale forces like gravity, pressure, and momentum, on the bulk flow and are usually intended to estimate the emplacement parameters from the dimensions, morphology and pre-existing slope of the flows. Such parameters include volumetric flow rate, duration of lava supply, flow advance rate, and rheologic characterizations of Newtonian or Bingham fluids. Although the rubbly channelized a`a flow shown in a 1a exhibits elements of randomness, the overall dynamics of the flow are governed by the systematic force of gravity and volume conservation between the active flow and the embanking levees [e.g., *Baloga et al*, 1998*; Glaze et al.,* 2009]. As a result, the list of models above use a deterministic approach that is appropriate for a`a flows such as that shown in Figure 1a. For a given boundary or initial condition, a deterministic model always produces the identical outcome. In the case of a lava flow, once the flow rate, rheology and slope are specified, a deterministic model will always produce exactly the same advance rate and flow depth as a function of time or distance.

The recognition of inflation in pahoehoe lava flows by *Hon et al.* [1994] revolutionized thinking about the style, pervasiveness, and importance of pahoehoe emplacement on the Earth, Mars, and Io [*Self et al.*, 1996, 1998; *Thordarson and Self,* 1998; *Keszthelyi et al.,* 1999, 2000, 2006]. In contrast to the a`a flow shown in Figure 1a, the pahoehoe deposit in Figure 1b is dominated by randomness in size, shape and orientation of individual volume elements (referred

44   to here as toes). This mode of flow emplacement is characterized by toe formation and inflation

45   [e.g., *Rowland and Walker,* 1990*; Hon et al.,* 1994 *Keszthelyi et al.,* 1999*; Baloga and Glaze,*

46   *2003; Harris et al., 2007; Keszthelyi et al.,* 2006; *Hamilton et al*., 2013]. High-resolution images

47   of lava flows on Mars indicate that both channelized a`a and pahoehoe styles of emplacement

48   may also occur in planetary environments (Figure 2). In the pahoehoe toe regime, stagnation,

49   inflation, and toe formation are most closely tied to the final topography, dimensions, and

50   morphologic features. The combination of low slopes and low flow rates typical of pahoehoe

51   emplacement results in minimal disruption of a rapidly forming, insulating crust [*Hon et al.,*

52   1994]. The efficient crustal insulation limits cooling to conduction only, allowing the interior

53   lava to remain fluid for long periods of time in contrast to a`a flows where fresh lava is

54   continuously exposed at the surface [e.g., *Crisp and Baloga,* 1990; *Wright and Flynn,* 2003,

55   *Wright et al*., 2011].

56   Although the forces of gravity, pressure and momentum are present in pahoehoe

57   emplacement, other influences act on each individual volume element, or parcel, of lava with a

58   randomizing effect. The mechanical strength of the cooling surface, pressure, crystallization,

59   micro-topography (i.e., centimeter-scale relief) and similar factors cause non-gravitational forces

60   to dominate the dynamics of emplacement. These forces at the parcel-scale are subject to natural

61   variations that necessitate an approach, different from the classical deterministic models, that

62   accounts for ubiquitous random effects and inflation.

63   In current practice, models of a`a flows are generally set up by considering the forces that act

64   on control volumes that slice through the flow from the underlying surface to a height

65   characteristic of the entire flow depth. In theory, one could divide a large lava flow up into tiny

66   volume parcels and consider the effects of these forces on each volume element. However, for

67   large flows (e.g., channelized a`a flows), such an approach significantly increases computational

68   complexity without adding significant new information. The essential effects of fluid flow are

69   retained when one considers a volume element that is equal to the full thickness and width of the

70   flow (a control volume up to many tens of cubic meters).

71   For pahoehoe flows that are dominated by random effects, the scale has been set in recent

72   works at a parcel scale typical of an individual toe [*Glaze and Baloga*, 2013], with a volume of

73    $0.75 \times 0.66 \times 0.2$ m^3 [Crown and Baloga, 1999]. At this scale, a parcel at the surface of a lobe is

74   subject to many forces with random effects.   These include forces associated with cooling,

75   cracking, rupturing, stretching and various forces from neighboring parcels on the surface and

76   beneath the parcel. A parcel in the interior of a lobe may be influenced by forces associated with

77   internal processes such as crystallization and vesiculation, and external forces from neighboring

78   parcels with a different rheology, momentum, shear state, crystal content and ultimately the

79   propagated influence of the underlying lobe topography and the mechanical strength of the crust

80   and visco-elastic layers. Thus, for a pahoehoe lobe, the behavior of the individual parcels (at the

81   scale of a typical toe) must be considered and then aggregated together to understand the overall

82   properties of the entire lobe.

83   The fundamental difficulty in developing a new model for pahoehoe lava flows is that the

84   random effects associated with inflation, internal fluid pressure, and crustal strength dominate

85   the emplacement [*Hon et al.* 1994*; Thordarson and Self,* 1998*; Keszthelyi et al.,* 1999*; Crown*

86   *and Baloga, 1999; Baloga and Glaze, 2003; Harris et al., 2007; Glaze and Baloga, 2013].*

87   Thus, in contrast to a deterministic approach, a model that includes random effects produces a

88   distribution of outcomes for the same given boundary or initial conditions. In the case of a lava

89   flow with the same specification of flow rate, rheology and slope as a deterministic model, each

90   run (or simulation) of a random model will result in a slightly different advance rate and flow

91   depth as a function of time or distance.

92   When many runs of a random model are performed, the suite of advance rates and flow depths

93   results in a distribution of these variables with some mean values and dispersions. Assuming the

94   basic physics is the same for these two types of approaches, one would presume that the mean

95   values of the random model approach those of the deterministic model if enough random

96   simulations are performed.

97   The key point is that there is uncertainty associated with the outcomes of a random model.

98   With only one run, there is no way to determine whether a particular simulation has produced an

99   outcome near the mean value or something that is rather unlikely. This can only be determined

100   by acquiring enough simulations to gauge the dispersion of the outcomes.

101   *Baloga and Glaze* [2003] developed an initial 2-dimensional model for pahoehoe

102   emplacement based on classical uncorrelated and correlated random walks [*Chandrasekar*,

103   1943]. They showed that a wide variety of field observables could be explained by such an

104   approach. The topographic profiles of simple lobes, the tendency for central channel

105   development, frontal steepening and similar pahoehoe manifestations were broadly in agreement

106   with field observations. However, the computational requirements for further advances at that

107   time were intractable.

108   *Glaze and Baloga* [2013] presented a more comprehensive model that simulated random

109   transfers of individual lava parcels within a pahoehoe lobe as a function of space and time. The

110   model was based on volume conservation and a set of probability rules for the parcel transfers.

111   The output of the model (Figure 3) was 3-dimensional topography that showed how the lobe

112   thickened and expanded with time subject to a variety of factors such as the source geometry,

113   confining barriers, and volumetric flow rate. Of particular interest was the degree of lobe

114   inflation, i.e., the degree to which the existing lobe thickens at the expense of expansion at the

115   margins. The basic model described in *Glaze and Baloga* [2013] assumes that all occupied basal

116   locations are equally likely to be the site of the next parcel transfer and is referred to here as the

117   'equiprobable' model.

118   The statistical concept of correlation [*Sheskin*, 1997] in lava transfers (i.e., the statistical

119   dependence of one lava parcel movement on another) was also explored by *Glaze and Baloga*

120   [2013]. Correlation in the lava transfers at the margin was shown to have a significant effect on

121   the lateral expansion, the thickness profiles and the rate of expansion of the lobe. However,

122   plausible physical causes for the correlation were addressed only in general terms.

123   The most obvious physical process omitted from the earlier models was the cooling of the

124   outer surface of the lobe. The primary issue is the extent to which such cooling would influence

125   the morphology, dimensions and inflation of the lobe. Another physical process omitted from

126   the earlier models is the role of the internal fluid pressure. The simulations of *Glaze and Baloga*

127   [2013] clearly showed local topographic highs and lows within the lobe that would pressurize all

128   connected parts of the hot mobile fluid interior. Thus one might expect topographic gradients to

129   influence breakouts in remote parts of the lobe as is often observed in the field.

130   In this work the explicit cooling of surface parcels has been added to the simulation approach

131   Glaze *and Baloga* [2013]. The temperature of the surface units is modeled by Hon's surface

132   cooling formula [*Hon et al*., 1994]. The probability rules of *Glaze and Baloga* [2013] have been

133   modified to increase the probability of a transfer when the surface temperature is relatively high

134   and decrease transfer probabilities for cooler parcels. Simulations of this process are referred to

135   as the 'temperature-dependent' model.

136   Another modification of the probability rules of *Glaze and Baloga* [2013] addresses the

137   influence of inflation within the lobe, resulting in a third distinct type of simulation. Inflation is

138   defined here as an increase in lobe volume with no concurrent increase in lobe area. Internal

139   transfers within an existing lobe result in a local inflation that produces topographic high points.

140   Basic physics considerations suggest that the increase in lobe thickness causes an increase in the

141   pressure throughout all connected parts of the fluid interior, whether near the topographic high or

142   not. Such an increase in pressure increases the probability of a breakout at the mechanically

143   weaker confining locations of the lobe. The third type of simulation in this work forces breakouts

144   to occur at the weaker locations of the lobe as governed by the cooling of the surface units.

145   Simulations of this process are referred to as the 'pressure-dominated' model. Opportunities for

146   future theoretical and field studies are given in conclusion.

147

148   **2. The Simulations**

149   The term 'simulation' in this work means specifically that one or more of the input quantities

150   of the simulation is a random variable. In a simulation, a particular value of each random

151   variable is drawn from a prescribed probability distribution. Each simulation represents a single

152   trial or 'realization' of all the output observables at the end of the simulation. Due to

153   randomness, each simulation produces a different set of outcomes depending on the nature of the

154   underlying probability distributions. Use of this simulation approach allows exploration of the

155   range of expected outcomes for each case of prescribed probabilities.

156   Each of the three simulation cases examined here ('equiprobable', 'temperature-dependent',

157   and 'pressure-dominated') is based on different sets of probabilistic rules for lava transfers that

158   are based on different physical considerations. All simulations assume a flat pre-existing surface,

159 with a constant rate of lava supply, where each parcel volume of 0.09 m^3 is equal to a typical

160 pahoehoe toe (see *Glaze and Baloga* [2013] for more details on the basic model). Because the

161 volume of a lava parcel is fixed, the volumetric supply rate can be adjusted by simply changing

162 the time interval between parcel additions at the source. A time interval of 15 seconds is used in

163 the results presented below, based on average volume supply rates observed for a small (< 10.4

164 m^3) toe lobe in Hawaii [*Hamilton et al.*, 2013]. Time varying and fluctuating supply rates can be

165 modeled by modulating the time interval between parcel additions at the source. Such analyses

166 are reserved for future analyses.

167

168 **2.1. Equiprobable Simulations.**

169   In the equiprobable case, the probability of a transfer of lava at each time step of the

170 simulation is considered to be a constant for all basal locations within a lobe that are occupied by

171 at least one lava parcel [*Glaze and Baloga*, 2013]. There are two random selections by the

172 algorithm at each time step. The first determines the basal cell location that will be the source of

173 the next transfer. The second determines the direction of the next transfer from the source

174 location (i.e., north, south, east or west). The dimensions and morphology of the lobe are

175 updated with each time step. A comprehensive description of this type of simulation is given in

176 *Glaze and Baloga* [2013].

177   The simulated equiprobable lobe shown in Figure 3 assumes a single parcel as the lobe

178 source, and subsequent release of 2500 additional lava parcels. Using 0.09 m^3 as the typical

179 volume of an individual toe [*Crown and Baloga*, 1999], the total volume of the lobe is 225 m^3.

180 This is consistent with the range of volumes reported in field studies of lobes emplaced

181   predominantly in the toe regime [*Crown and Baloga,* 1999; *Baloga and Glaze*, 2003; *Hamilton*

182   *et al.,* 2013].

183

184   **2.2. Temperature-Dependent Simulations.**

185   Ultimately, the mechanical strength of the crust controls the movement of lava within the lobe

186   and at its margins. The surface temperature is taken here as a proxy for the mechanical strength

187   of the crust. The surface cooling rates of pahoehoe lavas are well known, both from theoretical

188   and empirical studies [e.g., *Harris and Baloga*, 2009; *Crisp and Baloga*, 1990; *Hon et al.*, 1994;

189   *Wright and Flynn*, 2003]. The fundamental assumption of the temperature-dependent approach

190   is that warmer parcels are more likely to be the site of the next transfer than cooler ones.

191   Specifically, it is assumed that the probability of a lava parcel transfer at a particular location is

192   directly proportional to the temperature of the surface parcel at that location. Mathematically, the

193   probability that basal location j at time t is the site of the next parcel transfer is

194    $$P_j(t) = \frac{T_j(t)}{\sum\limits_{i} T_i(t)}$$ (1)

195   where $T_j(t)$ is the temperature of the surface at location j and the i summation is taken over all

196   occupied basal locations at time t. Once the location for the lava transfer has been determined by

197   (1), the current algorithm treats the four possible directions for the lava transfer as equiprobable.

198   The simulations assume that a parcel of lava begins to cool when a cell is first occupied and

199   thus exposed to the atmosphere. Other parcels may be transferred to that cell location, but are

200   assumed to increase the volume (inflate) at that location, keeping the original cell on the surface

201   to continue cooling. The empirical formula of *Hon et al.* [1994] is used to cool each surface

202   parcel separately for each time step of the lobe emplacement.

203 $$T(t) = -60.8 \ln(t) + 303 \qquad\qquad\qquad (2)$$

204   where t is measured in hours and T is given in $^{\circ}$C.

205   In the present model, internal transfers only inflate the lobe locally and leave the pre-existing

206   crust undisturbed and continuing to cool. Heat is propagated through the crust very slowly [e.g.,

207   *Crisp and Baloga*, 1990; *Harris and Rowland*, 2001]. Thus, it is assumed that only the surface

208   parcels (20 cm thick) cool to any significant degree. For the emplacement times considered here

209   (1/2 – 5 hours) the thermal boundary layer penetrates only to a few cm or less (*Hon et al.*, 1994,

210   e.g., Figure 10; *Crisp and Baloga*, 1990)

211   The thermal properties of basaltic crust that insulate the fluid interior have been documented

212   for many years (e.g., *Peck*, 1978; *Crisp and Baloga*, 1990; *Lipman and Banks*, 1987; *Moore*,

213   1987; *Hon et al.*, 1994). Thus in this work the interior parcels are assumed to remain at a

214   constant temperature (~1140 $^{\circ}$C [*Lipman and Banks*, 1987]) until they break out into an

215   unoccupied cell at the existing margin of the lobe. The initial surface temperature of a breakout

216   at the margin (occupation of a new cell location) is set to 1140 $^{\circ}$C no matter when it occurs in the

217   simulation. Subsequently the breakout parcel cools according to the formula of *Hon et al.* [1994].

218   Figure 4 shows the *Hon et al.* [1994] cooling curve for a time period of 24 minutes. For a

219   lobe with sixteen parcels, and 1.5 minute time steps (equivalent to an extremely low volume flow

220   rate used here for illustrative purposes only), the surface temperatures are indicated by the

221   arrows, where Parcel 1 (transferred at Time t_1) is the coolest, and Parcel 16 is the warmest.

222   In the temperature-dependent model, the probability for a parcel transfer is weighted by the

223   surface temperature. The probability distribution for determining which location will be selected

224   for the next parcel transfer is obtained by summing the temperatures of all surface parcels to

225   obtain a normalization at that particular time step. The assigned probability for a transfer at a

226 given location is simply the current surface temperature at that location divided by the

227 normalization at that time step. The example in Figure 5 illustrates the companion, normalized

228 probability (density) for the example in Figure 4, where the equiprobable case is also shown for

229 comparison.

230 Two typical 200-parcel examples of the temperature-dependent simulation are shown in

231 Figure 6. In these simulations, a parcel of lava volume was added to the lobe every 15 seconds,

232 such that the lobe was emplaced in 50 minutes. Although there is a great deal of variability and a

233 number of complicating factors (e.g., changes in topography, lava supply rate), such an

234 emplacement time is reasonably consistent with a lobe volume of 18 m^3 (200 parcels $\times$ 0.09m^3).

235 The general topography and morphology of these lobes is very similar to the equiprobable

236 case. The physical basis for this is that the cooling of the surface parcels is so rapid that most

237 parcels are on the long flat end of the cooling curve (Figure 4) and thus have roughly the same

238 probability of a transfer. There is a slight difference however, as suggested by the elevated

239 surface temperatures at the margin.

240 A measurable quantity of interest is the maximum extent of the lobe from the source. This

241 distance is denoted as r_{max}. To compare the temperature-dependent and equiprobable cases, 300

242 simulations were done for each approach. For each individual simulation the maximum distance

243 from the source was computed for a lobe of 200 parcels. The results are shown in Figure 7a. The

244 shape of the distribution of r_{max} in both cases is very similar to a lognormal distribution. The

245 temperature-dependent simulations have a slightly higher mean value, meaning that the

246 temperature-dependent cases tended to travel somewhat farther than the equiprobable cases.

247 Given the great degree of variability (i.e., the high standard deviations) of both simulation

248 approaches it is highly unlikely that these two emplacement scenarios could be distinguished in

249   the field. Moreover, there are a host of other complicating factors, such as variations in pre-

250   existing topography, lava supply and so forth that would complicate the discrimination.

251

252   **2.3. Pressure-Dominated Simulations.**

253   These simulations extend the temperature-dependent algorithm by including the influence of

254   internal fluid pressure increases due to inflation. When there is an internal lava transfer to a

255   location within the lobe the thickness at that location increases. This local inflation increases the

256   fluid pressure not only at that location, but also at all connected fluid locations within the lobe.

257   This is similar to inflating a balloon with various mechanical strengths at different parts of its

258   surface.

259   The pressure-dominated algorithm captures the influence above by using a combination of

260   random and systematic influences on the parcel transfers. When there are no internal transfers

261   (and thus no inflation), the location of the next breakout is determined randomly from the

262   probabilities derived from the local surface temperatures, i.e., fresh locations have a higher

263   probability than older ones (identical to the temperature-dependent case). However, the rules

264   change somewhat after there have been internal transfers (Figure 8). After one or more internal

265   transfers, there will eventually be a 'breakout' where a parcel will be transferred to a previously

266   unoccupied cell. When this happens, the pressure-dominated model assumes that the build up of

267   pressure results in the systematic selection of the last breakout location as the source in the next

268   time step and only the direction of the subsequent breakout is chosen at random.

269   The inclusion of inflation pressure in this way has a dramatic effect on the morphology and

270   dimensions of the lobe particularly its plan form shape and maximum length (Figure 9). The

271   pressure influence in the algorithm provides a statistical correlation, i.e., a systematic effect

272   imposed on the randomness. Such correlations were suggested in *Baloga and Glaze* [2003] and

273   *Glaze and Baloga* [2013], but were only vaguely attributed to possible physical causes. Here the

274   correlations in lava transfers are specifically attributed to an increase in the hydrostatic pressure

275   within the lobe and a temperature-dependent weakness at the margin.

276   The pressure-dominated simulations have a distinct lobate morphology that is markedly

277   different from the more axisymmetric equiprobable and temperature-dependent simulations. The

278   examples in Figure 9 show the concentration of warmer parcels toward the front of the

279   advancing lobes. In particular, it is interesting to compare Trial 2 to the equiprobable and

280   temperature-dependent cases. Despite the extent of the flow being similar to the equiprobable

281   and temperature-dependent simulations, the surface temperature distribution is quite different

282   from those in Figure 6. The pressure-dominated simulations show a very marked directionality

283   with the warmer parcels clustered at the end of the lobe, even though the flow has wrapped

284   around on itself, whereas the temperature-dependent lobes have warm parcels distributed along

285   the entire margin of the lobe.

286   The distribution of maximum distances from the source is shown in Figure 7b for 300

287   simulations of 200 parcels each at 15 second intervals. The mean value of r_{max} is now 13.2

288   parcels, almost double the equiprobable and temperature-dependent cases. Because the total

289   volume of all the simulations has been held fixed, the greater length of these lobes gives a much

290   thinner overall thickness as noted in *Glaze and Baloga* (2013).

291   Despite the more lobate plan form and relatively smaller thicknesses, the pressure-dominated

292   lobes exhibit comparable degrees of inflation, retaining this ubiquitous pahoehoe emplacement

293   characteristic. Figure 10 shows the rate of inflation for a typical equiprobable reference case

294   versus two typical examples of the pressure-dominated case, all with 200 parcel simulations. It is

295 readily seen that the overall vertical growth the lobe is essentially the same. Unlike the

296 morphology and extent of the lobe, this aspect of emplacement cannot be used to distinguish the

297 underlying physical processes.

298

299 **3. Conclusions.**

300 This work shows that the cooling of the surface alone has little influence on the morphology,

301 dimensions and the rates of lateral expansion and inflation compared to the equiprobable,

302 temperature-independent simulations of *Glaze and Baloga* [2013]. Lobes with surface parcels

303 that cool according to Hon's formula [*Hon et al.*, 1994] retain the approximate Gaussian

304 topography and symmetric plan form identified by field observations and the earlier temperature-

305 independent simulations [*Crown and Baloga*, 1999; *Baloga and Glaze* 2003; *Glaze and Baloga*,

306 2013]. The differences in morphology, dimensions, aspect ratios, and maximum extents from the

307 source for lobes with cooling and constant temperature surface units are so slight they are

308 unlikely to be distinguishable in the field. Such a result might be anticipated intuitively for this

309 emplacement regime (e.g., 200 parcels released at 15 second intervals) because radiative cooling

310 is so rapid that most locations within the lobe have approximately the same probability for an

311 internal lava transfer or breakout at the margin.

312 When the internal inflation pressure originally identified by *Hon et al.* [1994] causes

313 systematic breakouts at the warmest (and therefore weakest) margins, the morphologies and

314 dimensions of the simulated lobes are dramatically different from the purely temperature-

315 dependent and equiprobable cases. The internal fluid pressure due to inflation is felt uniformly

316 with all contiguous fluid regions within a lobe so that the warmest and weakest margins become

317 the most likely locations for margin expansion. This is a physical explanation for the correlations

318 considered in *Baloga and Glaze* [2003] and *Glaze and Baloga*, [2013]. Both works concluded

319 that correlation was required to explain a variety of observed lobe features such as directionality,

320 aspect ratio, topographic cross-lobe profiles and the tendency to form channels and embanking

321 levees.

322 It is the combination of inflation pressure and the mechanical weakness of the warmer and

323 weaker margins that causes lobes to become significantly more elongate than their temperature-

324 dependent and equiprobable counterparts. The overall thickness and plan form shapes of lobes

325 formed by this process are readily distinguishable from the temperature-dependent and

326 equiprobable cases. The evolving surface temperature distributions of the pressure-dependent

327 lobes are also readily distinguishable from the purely temperature-dependent and equiprobable

328 cases. It is noteworthy, however, that the time-dependent rate of inflation remains essentially the

329 same in all cases.

330 The types of simulations performed in this work offer the promise of developing quantitative

331 inferences about emplacement conditions from the dimensions and morphologies of pahoehoe

332 lobes that were not observed while they were active. Comprehensive field campaigns for active

333 lobes with a range of local discharge rates are needed to identify the appropriate model for

334 detailed data-theory comparisons. These measurements should include pre-existing topography,

335 time-series changes in flow morphology, and thermal imaging. This would permit isolation of

336 the different physical processes governing the shape and dimensions of the lobe and a statistical

337 characterization of the random effects. The next steps in advancing these models are the

338 incorporation of an underlying regional slope and the influence of micro-topography. Such

339 advances would provide a methodology for developing quantitative inferences about the

340 unobserved emplacement of terrestrial and planetary pahoehoe lava flows.

341

4. Acknowledgements.

348

349   **REFERENCES**

350   Baloga, S.M., Lava flows as kinematic waves, J Geophys Res, 92(B9), 9271-9279, 1987.

351   Baloga, S., and L.S. Glaze, Pahoehoe transport as a correlated random walk, J Geophys Res, 108

352   (B1), 2031, doi:10.1029/2001JB001739, 2003.

353   Baloga, S., and L.S. Glaze, Self-replication model for long channelized lava flows on the Mars

354   plains, J Geophys Res, 113, E05003, doi:10.1029/2007JE002954, 2008.

355   Baloga, S.M., P.D. Spudis, and J.E. Guest, The dynamics of rapidly emplaced terrestrial lava

356   flows and implications for planetary volcanism, J Geophys Res, 100 (B12), 24509 - 24519,

357   1995.

358   Baloga, S., L.S. Glaze, D. Crisp, and S.A. Stockman, New statistics for estimating the bulk

359   rheology of active lava flows: Puu Oo examples, J Geophys Res, 103, 5133-5142, 1998.

360   Baloga, S.M., L.S. Glaze, M.N. Peitersen, and J.A. Crisp, Influence of volatile loss on thickness

361   and density profiles of active basaltic flow lobes, J Geophys Res, 106 (B7), 13,395 -

362   13,405, 2001.

363   Chandrasekhar, S., Stochastic problems in physics and astronomy, Reviews of Modern Physics,

364   15, 1 – 87, 1943.

365   Crisp, J.A. and S.M. Baloga, A model for lava flows with two thermal components, J Geophys

366   Res, 95, 1255-1270, 1990.

367   Crown, D.A., and S.M. Baloga, Pahoehoe toe dimensions, morphology, and branching

368   relationships at Mauna Ulu, Kilauea Volcano, Hawaii, Bull Volcanol, 61, 288-305, 1999.

369   Danes, Z.F., Dynamics of lava flows, J Geophys Res, 77, 1430-1432, 1972.

370   Glaze, L.S. and S.M. Baloga, 2013, Simulation of inflated pahoehoe lava flows, J Volcanol

371   Geotherm Res, 256, 108-123, doi:10.1016/j.jvolgeores.2013.01.018, 2013.

372   Glaze, L.S., S.M. Baloga, W.B. Garry, S.A. Fagents, and C. Parcheta, A hybrid model for leveed

373   lava flows: Implications for eruption styles on Mars, J Geophys Res, 114, doi:

374   10.1029/2008je003278, 2009.

375   Glaze, L.S., S.M. Baloga, S.A. Fagents, R.Wright, The influence of slope breaks on lava flow

376   surface disruption, J Geophys Res, 119, doi:10.1002/2013JB010696, 2014.

377   Hamilton, C.W., Glaze, L, James, M.R., and S.M. Baloga, Topographic and stochastic influences

378   on pāhoehoe lava lobe emplacement, Bull Volcanol, 75, 756, 2013.

379   Harris, A.J.L. and S.M. Baloga, Lava discharge rates from satellite-measured heat flux,

380   Geophysical Research Letters, 36 (L19302), doi:10.1029/2009GL039717, 2009.

381   Harris, A.J.L., and S.K. Rowland, FLOWGO: A kinematic thermo-rheological model for lava

382   flowing in a channel, Bull Volcanol, 63, 20–44, 2001.

383   Harris, A.J.L., J. Dehn, M.R. James, C. Hamilton, R. Herd, L. Lodato, and A. Steffke, Pahoehoe

384   flow cooling, discharge, and coverage rates from thermal image chronometry, Geophysical

385   Research Letters, 34 (L19303), doi:10.1029/2007GL030791, 2007.

386   Harrison, C.G.A., and C. Rooth, The dynamics of flowing lavas, in Volcanoes and

387   Tectonosphere, edited by H. Aoki and S. Iizuka, pp. 103-113, University of Tokyo, Tokyo,

388   1976.

389   Hon, K., J. Kauahikaua, R. Denlinger, and K. Mackay, Emplacement and inflation of pahoehoe

390   sheet flows: Observations and measur4ments of active lava flows on Kilauea Volcano,

391   Hawaii, Geol Soc Am Bull, 106 (3), 351-370, 1994.

392   Keszthelyi, L., S. Self, and T. Thordarson, Application of recent studies on the emplacement of

393   basaltic lava flows to the Deccan Traps, Memoirs – Geol Soc India, 43, 485-520, 1999.

394   Keszthelyi, L., A.S. McEwen, and T. Thordarson, Terrestrial analogs and thermal models for

395   Martian flood lavas, J Geophys Res, 105 (E6), 15,027-15,049, 2000.

396   Keszthelyi, L., S. Self, and T. Thordarson, Flood lavas on Earth, Io and Mars, J Geol Soc, 163

397   (2), 253-264, 2006.

398   Lipman, P.W. and N.G. Banks, AA flow dynamics, Mauna Loa 1984, USGS Prof Pap, 1350,

399   1527-1565, 1987.

400   Nichols, R.L., Viscosity of Lava, J Geo, 47, 290-302, 1939

401   Peck, D.L., Cooling and vesiculation of Alae lava lake, Hawaii, US Geol Surv Prof Pap 935-B,

402   1-59, 1978.

403   Rowland S.K. and G.P.L. Walker, Pahoehoe and aa in Hawai'i: volumetric flow rate controls the

404   lava structure, Bull Volcanol, 52, 615–628, 1990.

405   Rowland, S.K., A.J.L. Harris, and H. Garbeil, Effects of Martian conditions on numerically

406   modeled, cooling-limited channelized lava flows, J Geophys Res, 109 (E10010),

407   doi:10.1029/2004JE002288, 2004.

408   Self, S., T. Thordarson, L. Keszthelyi, G.P.L. Walker, K. Hon, M.T. Murphy, P. Long, and S.

409   Finnemore, A new model for the emplacement of Columbia River basalts as large, inflated

410   pahoehoe lava flow fields, Geophysical Research Letters, 23 (19), 2689-2692, 1996.

411   Self, S., L. Keszthelyi, and T. Thordarson, The importance of pahoehoe, Annual Reviews of

412   Earth Planetary Science, 26, 81-110, 1998.

413   Shaw, H.R., and D.A. Swanson, (1970), Eruption and flow rates of flood basalts. In Proceedings

414   2nd Columbia River Basalt Symposium, pp. 271-299, Eastern Washington State College

415   Press, Cheney.

416   Sheskin, D.J., Handbook of Parametric and Nonparametric Statistical Procedures, CRC Press,

417   719 pp., 1997.

418 Thordarson, T., and S. Self, The Roza Member, Columbia River Basalt Group: A gigantic

419   pahoehoe lava flow field formed by endogenous processes? J Geophys Res, 103 (B11),

420   27,411-27,445, 1998.

421 Wright, R. and L.P. Flynn, On the retrieval of lava-flow surface temperatures from infrared

422   satellite data, Geology, 31 (10), 893 – 896, 2003.

423 Wright, R., L. Glaze, and S.M. Baloga, Determining the eruption style and composition of

424   terrestrial lavas using hyperspectral satellite data, Geology, doi:10.1130/G32341.1, 2011.

425

426   Figures and Captions

(a)   (b)
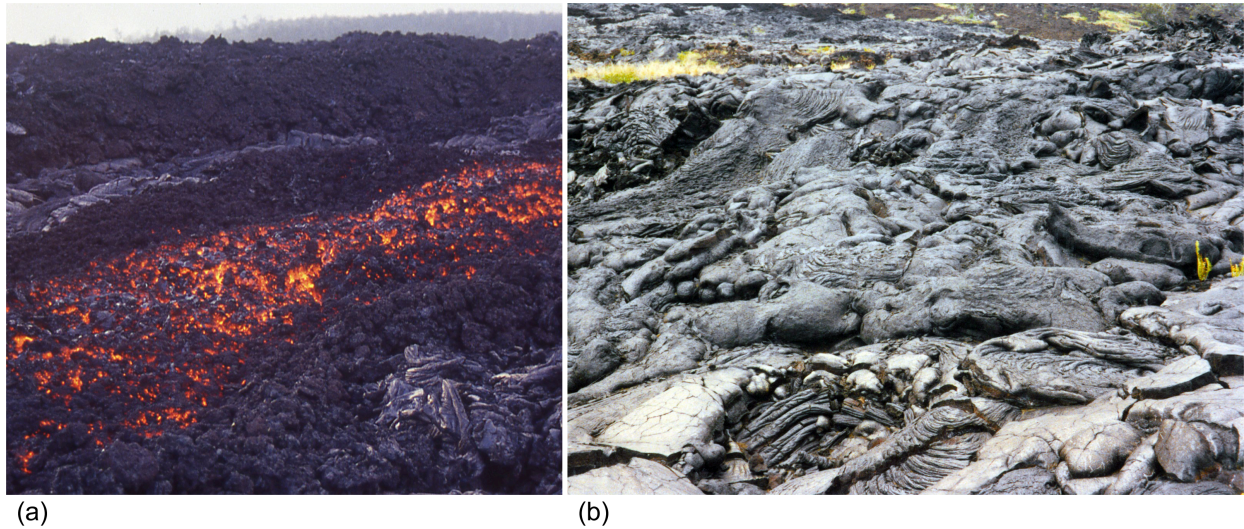
428   Figure 1: (a) Example active channelized a`a lava flow. The key morphologic feature of a`a lava

429   flows is the blocky surface. Indicators of lava transport processes are the raised levees along

430   the lateral flow margins and the central channel containing the flowing lava. Image used

431   with permission of S. Rowland.   (b) Field of pahoehoe toes. The key morphologic feature of

432   pahoehoe lava flows is the smooth, often ropy surface. The complexity of pahoehoe transport

433   and emplacement is illustrated by the randomness in dimensions and orientations of the lava

434   toes and lobes in this typical flow field.

435
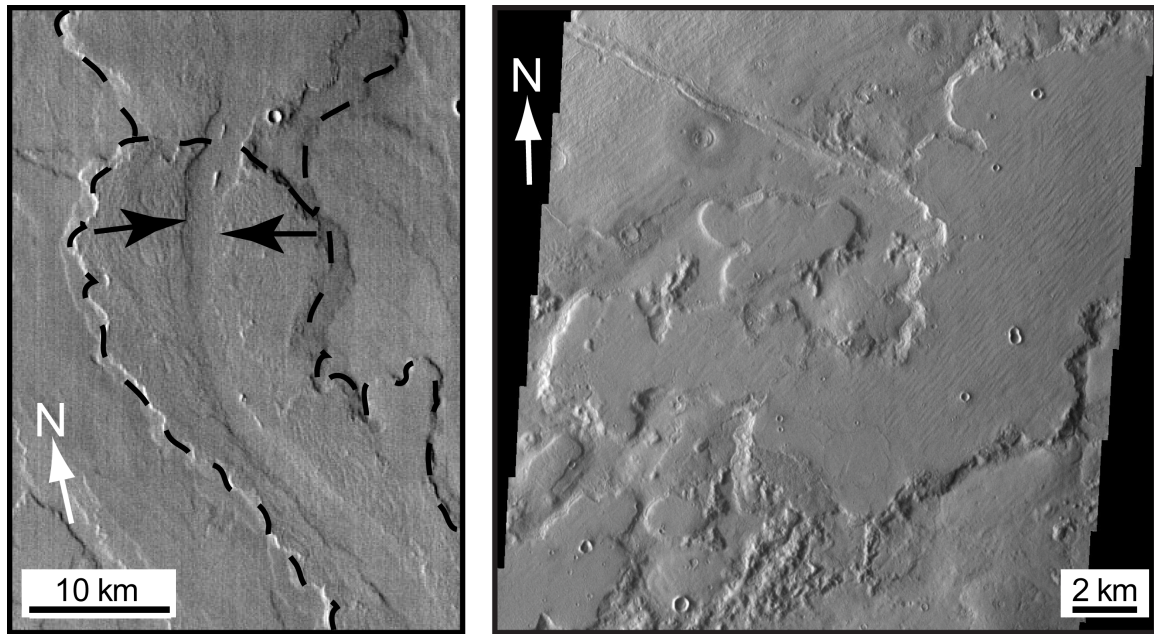
(a) N of Pavonis Mons   (b) NW of Elysium Mons

436

437   Figure 2: Examples of (a) a`a channelized flows and (b) putative pahoehoe lava flows on Mars.

438   The a`a flow is characterized by lateral levees (dashed line) and a well-established channel

439   (black arrows) for transporting lava to the flow front. The pahoehoe lava flow is

440   characterized by a broad flat surface that lacks any evidence of a channel, and that is

441   morphologically similar to terrestrial lava flows where pahoehoe lobes have coalesced to

442   form flat plateaus. The flow also exhibits margins with a great deal of variability analogous

443   to terrestrial flows that advance through pahoehoe toe lobes. Figure (a) is a Thermal

444   Emission Imaging Spectrometer (THEMIS) infrared image (frame I01739006). Figure (b) is

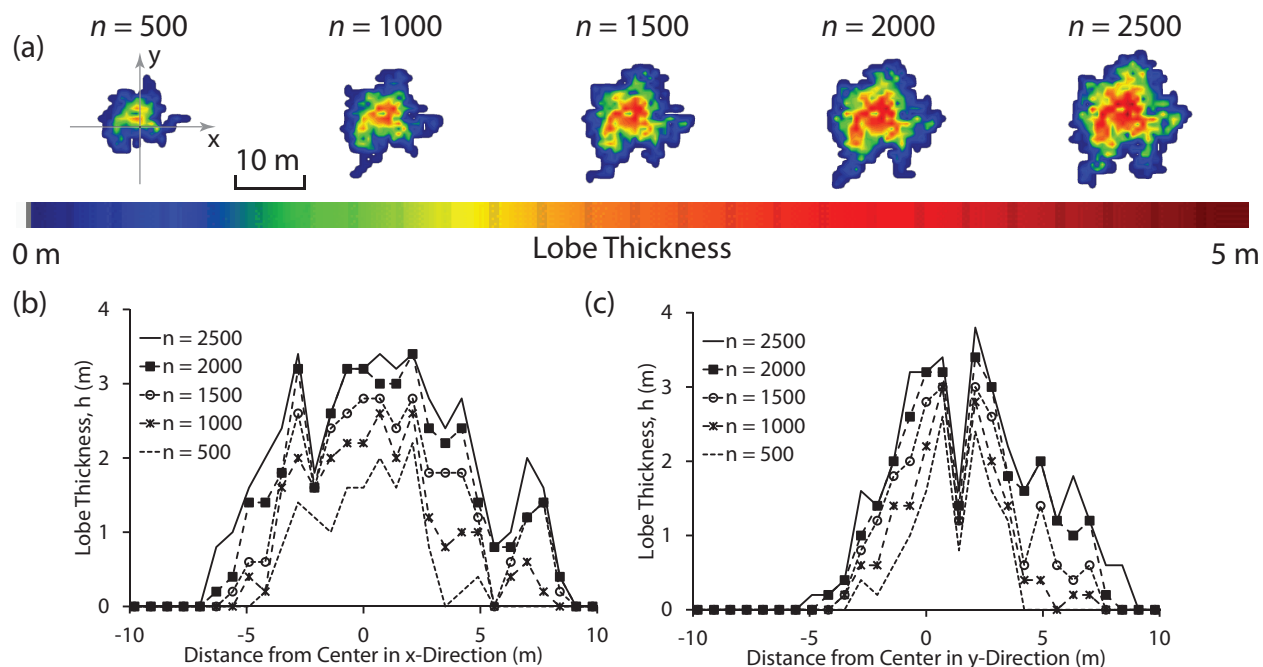445   a THEMIS visible image (frame V14162005).

446

447

448 Figure 3: Typical example of an equiprobable simulation. (a) 3-dimensional topography at five

449 time steps (n = 500, n = 1000, n = 1500, n = 2000, n = 2500). The source parcel location is

450 located at the intersection of the *x* and *y* axes. Corresponding cross-lobe topographic profiles

451 in the (b) *x* and (c) *y* directions are also shown. Generally the lobes are symmetric with the

452 variability in both plan form and topography being typical of field observations. Figure

453 reproduced with permission from *Glaze and Baloga* [2013].

454

The figure shows a plot with Temperature (°C) on the y-axis (0 to 1000) and Time (hours) on the x-axis (0 to 0.5). The red empirical model line is labeled:

$$y = -60.801\mathrm{Ln}(x) + 303$$
(Hon et al., 1994)

Arrows point upward at time steps labeled t_{16}, t_{13}, t_{10}, t_7, t_4, t_1.
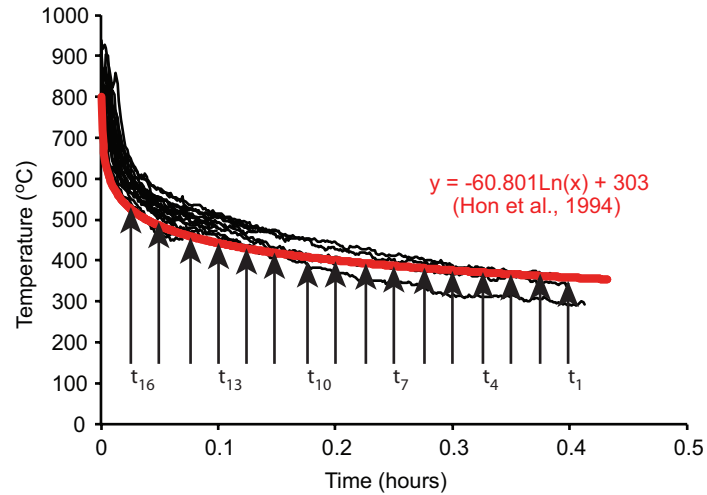
455

456   Figure 4: Pahoehoe surface cooling curves (black) adapted from *Harris and Baloga* [2009] and

457   empirical model (red) from *Hon et al*. [1994]. Model surface temperatures are indicated for

458   16 time steps (where each time step is 90 seconds and every parcel is exposed at the surface

459   for illustration purposes). The first parcel (time step 1) has been exposed at the surface for

460   0.4 hours (1440 s) and has the coolest surface temperature. The most recent parcel (time step

461   16) has only been exposed for 90 seconds and has the highest surface temperature.
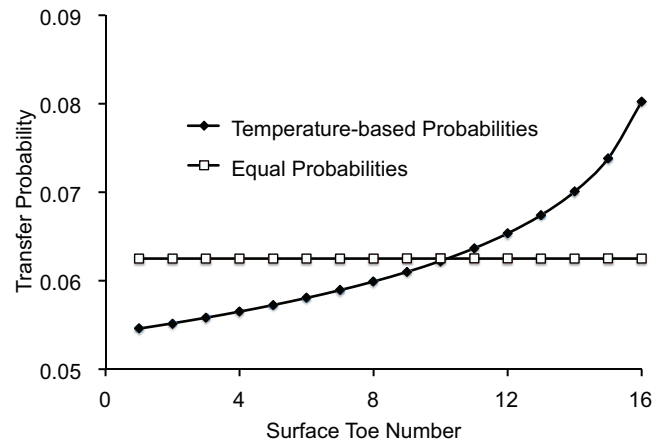
462

463

464   Figure 5:   Transfer probabilities for the temperature dependent model (solid diamonds)

465   corresponding to the time steps shown in Figure 4. Probabilities are directly correlated to the

466   surface temperature and the length of time a parcel has been exposed at the surface (all

467   parcels are exposed at the surface for this example). Toe 16 is the most recent parcel to be

468   exposed. Thus it has the highest surface temperature and the highest likelihood to be the

469   location of the subsequent parcel transfer. The equiprobable distribution is shown with open

470   squares for comparison.

471

Lobe Thickness   Surface Temperature

Trial 1

5 m

0 m   3.5 m   0 ℃   1140 ℃
(a)   (b)

Trial 2

5 m

0 m   3.5 m   0 ℃   1140 ℃
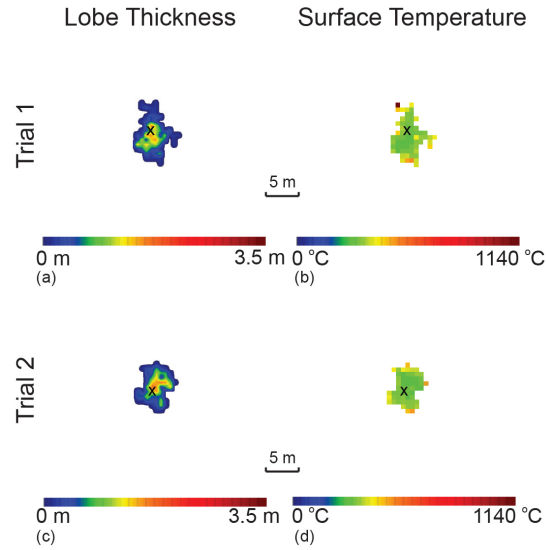(c)   (d)

472

473   Figure 6: Two example temperature-dependent simulations (Trials 1 and 2) with 200 parcels

474   each. The location of the initial parcel is indicated by an 'x'. In each Trial, the left panel

475   shows a smoothed representation of the lobe thickness, and the right panel shows the surface

476   temperature.
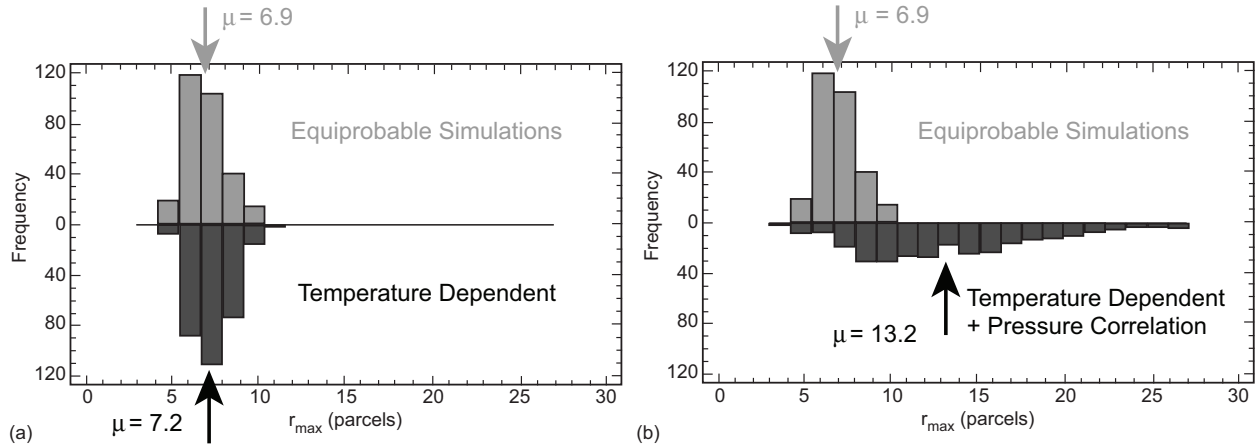
477

478 (a)

479   Figure 7: Distribution of maximum distance traveled (r_{max}) in 300 simulations. (a) Comparison

480   of r_{max} for 300 equiprobable simulations with 300 temperature-dependent simulations. (b)

481   Comparison of 300 equiprobable simulations to 300 simulations with both temperature

482   dependent probabilities and correlations based on increased pressure following internal

483   transfers.

484

(a) Two occupied margin cells

(b) Internal transfer locally inflates lobe and increases internal pressure

(c) Increased internal pressure drives new breakout

(d) Breakout after internal transfer releases pressure; next transfer occurs from breakout location; transfer directions are equally probable (= 0.25)

Available

(e) For this example, three of the four transfer options result in two cell locations available for the subsequent transfer

(f) The fourth transfer option results in an internal transfer, leaving only one location available for the subsequent transfer
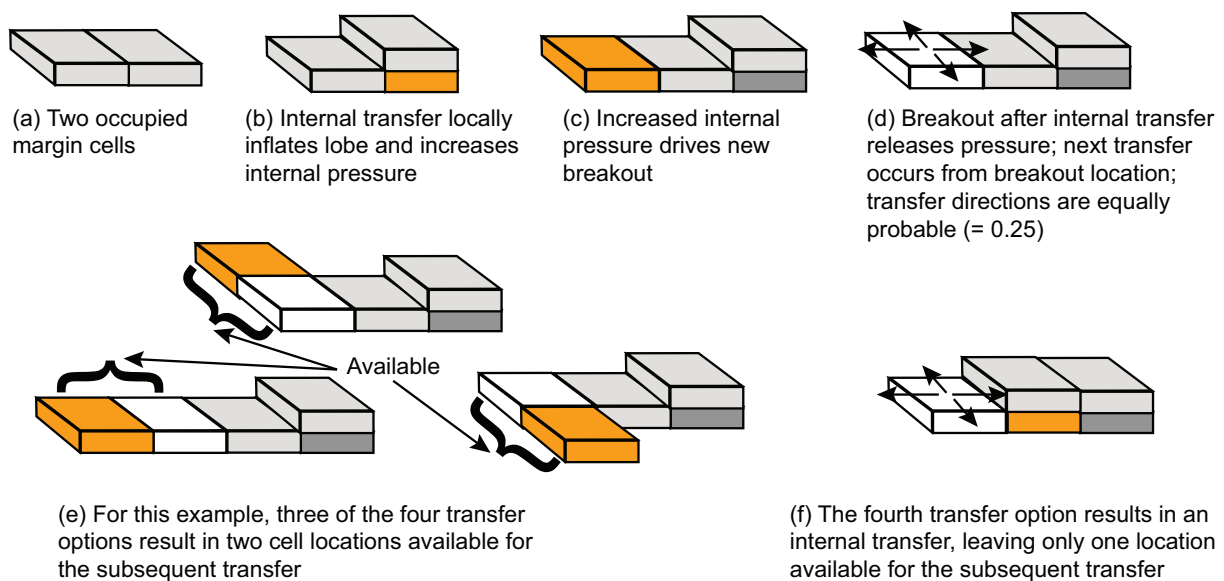
485

486   Figure 8: Cartoon illustrating the influence of pressure buildup at the location of two occupied

487   cells along the lobe margin (a) following inflation due to one or more internal parcel transfers

488   (b). Following a new breakout expanding the lobe's areal extent (c), only the most recently

489   occupied locations (weakest crust) are available for future parcel transfers (d – f). The net

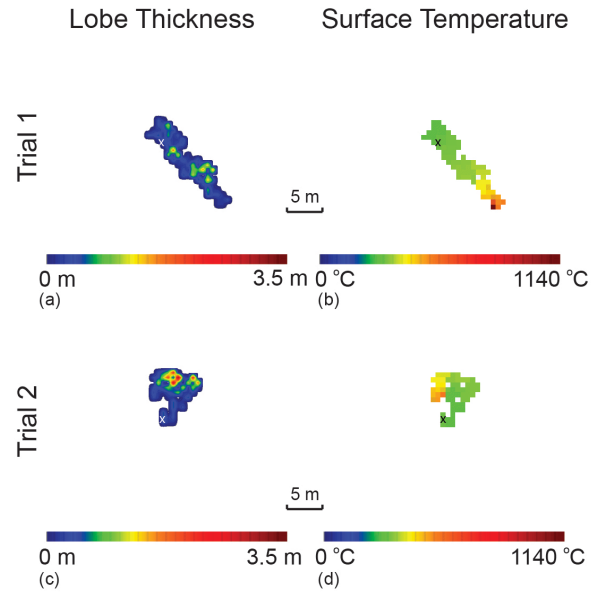490   result of the pressure effect is to elongate the planform shape of the lobe.

Figure 9: Two example simulations (Trials 1 and 2) with 200 parcels each with both temperature-dependent probabilities and pressure correlation. The location of the initial parcel is indicated by an 'x'. In each Trial, the left panel shows a smoothed representation of the lobe thickness, and the right panel shows the surface temperature.
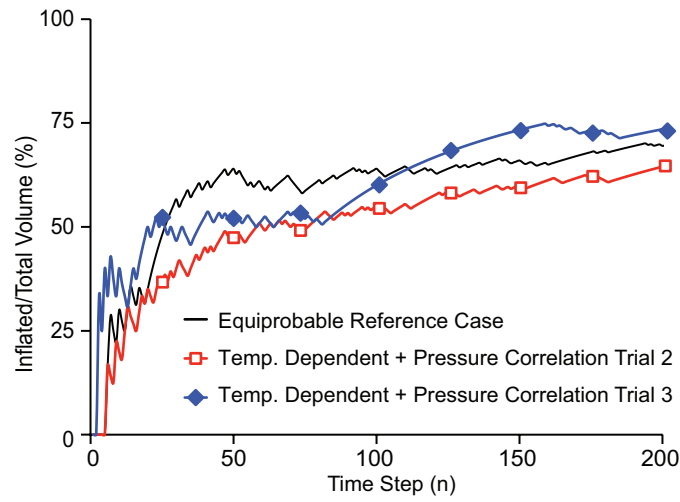
496

497   Figure 10: Three example simulations with 200 parcels each. The fraction of the total lobe

498   volume that is represented by internal parcel transfers (transfers that increase the lobe volume

499   without increasing the lobe area) is shown for the Equiprobable reference case as well as two

500   independent trials of the pressure-dominated case.